High-content microscopy and machine learning characterize a cell morphology signature of *NF1* genotype in Schwann cells

Jenna Tomkinson[1], Cameron Mattson[1], Michelle Mattson-Hoss[2], Herb Sarnoff[2], Stephanie J. Bouley[3], James A. Walker[3], Gregory P. Way[1,*]

[1]Department of Biomedical Informatics, University of Colorado School of Medicine
[2]Infixion Bioscience, Inc., San Diego, CA
[3]Center for Genomic Medicine, Massachusetts General Hospital, Harvard Medical School, Boston, MA, USA

*Corresponding Author: gregory.way@cuanschutz.edu

Abstract:

Neurofibromatosis type 1 (NF1) is a multi-system, autosomal dominant genetic disorder driven by the systemic loss of the NF1 protein neurofibromin. Loss of neurofibromin in Schwann cells is particularly detrimental, as the acquisition of a 'second-hit' (e.g., complete loss of NF1) can lead to the development of plexiform neurofibroma tumors. Plexiform neurofibromas are painful, disfiguring tumors with an approximately 1 in 5 chance of sarcoma transition. Selumetinib is currently the only medicine approved by the U.S. Food and Drug Administration (FDA) for the treatment of plexiform neurofibromas in a subset of patients. This motivates the need to develop new therapies, either derived to treat *NF1* haploinsufficiency or complete loss of *NF1* function. To identify new therapies, we need to understand the impact neurofibromin has on Schwann cells. Here, we aimed to characterize differences in high-content microscopy imaging in neurofibromin-deficient Schwann cells. We applied a fluorescence microscopy assay (called Cell Painting) to two isogenic Schwann cell lines, one of wildtype genotype ($NF1^{+/+}$) and one of *NF1* null genotype ($NF1^{-/-}$). We modified the canonical Cell Painting assay to mark four organelles/subcellular compartments: nuclei, endoplasmic reticulum, mitochondria, and F-actin. We utilized CellProfiler pipelines to perform quality control, illumination correction, segmentation, and cell morphology feature extraction. We segmented 22,585 *NF1* wildtype and null cells, utilized 907 significant cell morphology features representing various organelle shapes and intensity patterns, and trained a logistic regression machine learning model to predict the *NF1* genotype of single Schwann cells. The machine learning model had high performance, with training and testing data yielding a balanced accuracy of 0.85 and 0.80, respectively. All of our data processing and analyses are freely available on GitHub. We look to improve upon this preliminary model in the future by applying it to large-scale drug screens of NF1 deficient cells to identify candidate drugs that return NF1 patient Schwann cells to phenocopy NF1 wildtype and healthier phenotype.

Introduction:

Neurofibromatosis type 1 (NF1) is a haploinsufficient, autosomal dominant genetic condition that impacts approximately 1 in 3,000 individuals worldwide.[1–3] NF1 results from mutations in the *NF1* gene, with approximately half the affected individuals developing the disorder due to *de novo NF1* pathogenic variants.[4] The *NF1* gene encodes the protein neurofibromin, a GTPase-activating protein that negatively regulates Ras. Loss of NF1 results in increased Ras signaling effector and downstream pathways such as MAPK and mTOR signaling, which can cause unchecked cell proliferation.[5] Benign and malignant tumor development is connected to a "second hit" somatic mutation in the *NF1* gene, which results from a loss of heterozygosity (LOH) and additional mutations.[6,7] Generally, tumors are initiated by neurofibromin-deficient (*NF1*$^{-/-}$) Schwann cells, and driven by *NF1* haploinsufficient microenvironments.[1,2]

Over 99% of NF1 patients develop cutaneous neurofibromas (cNFs), benign skin tumors that significantly decrease quality of life.[8,9] Furthermore, about 30-50% of NF1 patients develop plexiform neurofibromas (pNFs), benign tumors that grow from nerves and are often painful and disfiguring. When surgically resected, 50% of pNFs regrow within 10 years.[10] Another 8-15% of NF1 patients have pNFs that transform into malignant peripheral nerve sheath tumors (MPNSTs), which are rare sarcomas that have a five-year survival rate that ranges greatly from patient to patient but can be as low as 16% or as high as 62%.[11,12] There is currently only one FDA-approved treatment for a subset of NF1 patients with pNFs called Selumetinib. This MEK1/2 inhibitor reduces tumor growth by suppressing MAPK signaling to reduce cell proliferation.[13] However, Selumetinib is only approved to treat pNFs (not MPNSTs), has limited efficacy of only 30-50% shrinkage of PNs in about half of patients, and many patients experience significant adverse events.[14,15]

We previously proposed the idea that therapeutically elevating neurofibromin activity in NF1 haploinsufficient Schwann cell environments will slow or reverse tumor development and other NF1 manifestations.[16] One way to identify treatments that therapeutically elevate neurofibromin is to screen many drugs that cause the desired effect. We and others have performed NF1 drug screening applications previously, but they either use cell types unrelated to NF1 and/or measure only simple readouts like cell viability or other endpoints that will not prioritize a drug that reverses specific phenotypes.[17–19] A revitalized approach, called phenotypic drug discovery, applies modern computational and microscopy tools to prioritize drugs based on their phenotypic effects on relevant cell models.[20] However, in order to pursue phenotypic drug discovery, we must first confirm feasibility and select an appropriate assay to identify a sensitive and specific phenotypic signature. Therefore, we aimed to demonstrate proof of concept that the under-utilized approach known as high-content microscopy can distinguish *NF1* genotype in Schwann cells. High-content microscopy, which enables scientists to extract rich phenotypic information directly from microscopy images of cells, has greatly evolved over the past twenty years, and it is now poised to accelerate its impact on many different diseases, including NF1.[21] Many studies have quantified molecular differences in Schwann cells with and without NF1[22–24]; however, few studies have quantified phenotypic differences. Kim et al., 1995, for example, analyzed phase-contrast micrographs of Schwann cells from each genotype, identifying that

complete neurofibromin loss (*NF1*$^{-/-}$) resulted in elongated cell processes and bright-refractile cell bodies as compared to wildtype cells (*NF1*$^{+/+}$).[25] While this study identified qualitative morphological differences, it was conducted through manual observation as opposed to an unbiased automatic system of quantitative data analysis. Here, we utilized modern advances in high-content microscopy to quantify cellular phenotypic variations at the single-cell level. We employed a modified version of the multiplex fluorescence microscopy assay called Cell Painting to mark four different organelles/subcellular compartments (nuclei, endoplasmic reticulum (ER), mitochondria, and F-actin cytoskeleton).[26] We used CellProfiler[27] to segment and measure quantitative cell morphology features in single cells.[28] We applied advanced image analysis and a machine learning pipeline to identify significant single-cell morphology differences in isogenic Schwann cells with different *NF1* genotypes (*NF1*$^{+/+}$ *and NF1*$^{-/-}$). Our high-content microscopy and machine learning approach predicts *NF1* genotypes with high performance, providing proof of concept that we can use phenotypic drug discovery to identify treatments that reverse NF1-deficient phenotypes. Furthermore, among these extracted cell morphology features, we identified endoplasmic reticulum and F-actin cytoskeleton that strongly differentiate *NF1* genotypes. This work sets the stage for future studies where pairing phenotypic drug discovery with machine learning can identify therapeutic agents that elevate wildtype neurofibromin levels, potentially slowing or reversing tumor development in NF1 patients.

Results:

Processing single-cell morphological profiles of Schwann cells

We applied our modified Cell Painting assay to mark nuclei, endoplasmic reticulum (ER), mitochondria, and F-actin of hTERT ipn02.3 2λ Schwann cells (*NF1*$^{+/+}$) and a CRISPR engineered isogenic null cell (*NF1*$^{-/-}$) (**Figure 1A**).[29] We employed image analysis and machine learning pipelines to extract, process, and analyze high-dimensional single-cell morphology features to identify an *NF1* genotype signature (**Figure 1B**). For our image analysis pipeline, we used CellProfiler to perform illumination correction to retrospectively correct uneven lighting across the images, including vignetting.[30] We then segmented nuclei, whole cells, and cytoplasm and extracted a total of 2,313 morphology features. We then applied image-based profiling[31], a method that formats morphological profiles to evaluate differences among cell populations. Specifically, we applied CytoTable to curate single-cell profiles[32] and pycytominer to annotate, normalize, select features, and aggregate these data in order to analyze downstream with machine learning.[33]

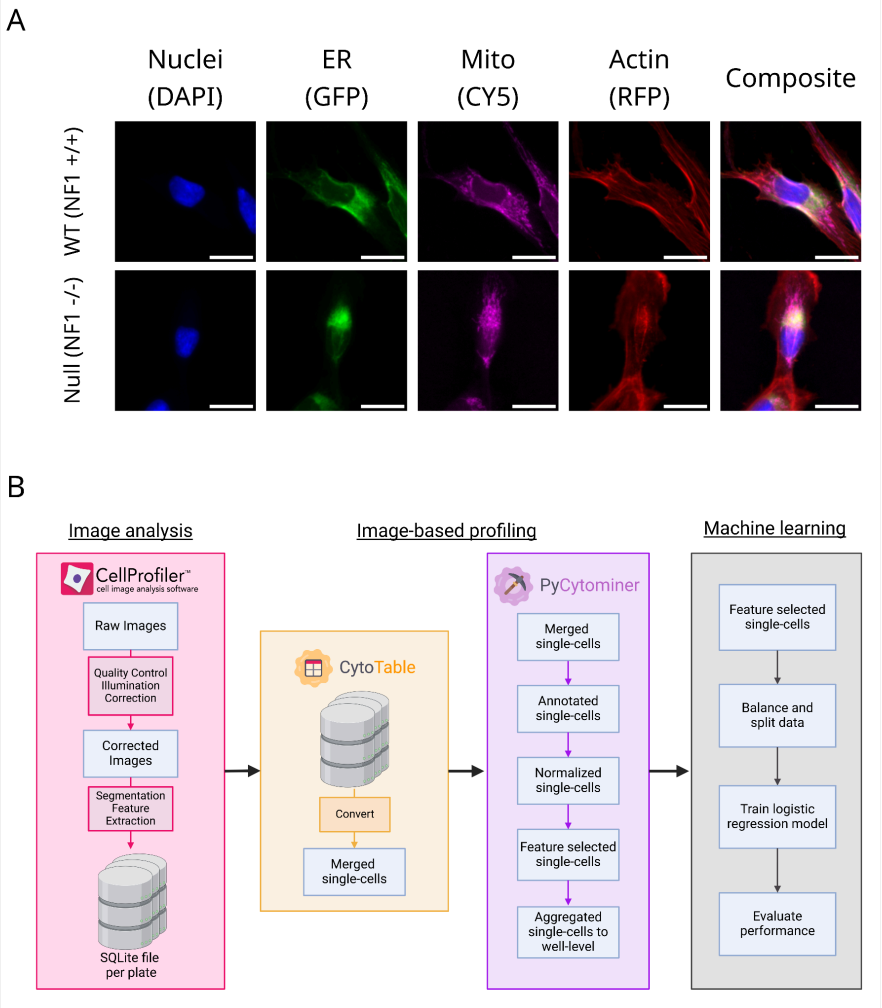

Figure 1. *Overview of Cell Painting and data analysis workflow*. (**A**) Example image montages of the Cell Painting channels and composite image (all channels overlayed) for each *NF1* genotype. The scale bar represents 25 μM. (**B**) The workflow of our analysis pipeline demonstrates the steps taken from image analysis to machine learning

We imaged and processed a total of 12,007 *NF1*$^{-/-}$ and 10,578 *NF1*$^{+/+}$ Schwann cells (22,585 total cells) (**Figure 2A**). We collected these cells across three 96-well plates (**Supplementary Figure 1A**; for plate maps, see **Supplemental Figure 2**). We applied a standard dimensionality reduction method called Uniform Manifold Approximation and Projection (UMAP)[34] to the single-cell morphology features and found that single cells were homogeneously clustered across both genotypes, indicating that if an *NF1* genotype signature was present, it manifests in only a few, subtle cell morphology features (**Figure 2B**). We did not observe clustering based on plate, indicating minimal or no batch effects (**Supplementary Figure 1B**). We aggregated the single-cell morphology features to the well-level of the plate, in which each well represents a single profile for all single cells. We calculated Pearson's correlations by comparing similar wells with either the same or different *NF1* genotypes. The mean correlation for the same genotype was r = 0.24, and the different genotype was r = 0.16. We performed a two-sample t-test which determined that these distributions are significantly different (t-statistic = 14.13, p-value = 6.78e-45) (**Figure 2C**). This result demonstrates a slight difference in morphology between

genotypes. We observed similar differences when looking at individual plates (**Supplementary Figure 1C**). Overall, these results suggest that the morphological differences between *NF1* genotypes are subtle at both the single-cell and well-population level. We expected this result given *NF1* genotype is the only difference in this otherwise isogenic cell line. We next demonstrated the ability to detect these differences by training a machine-learning model to classify single-cell *NF1* genotypes.

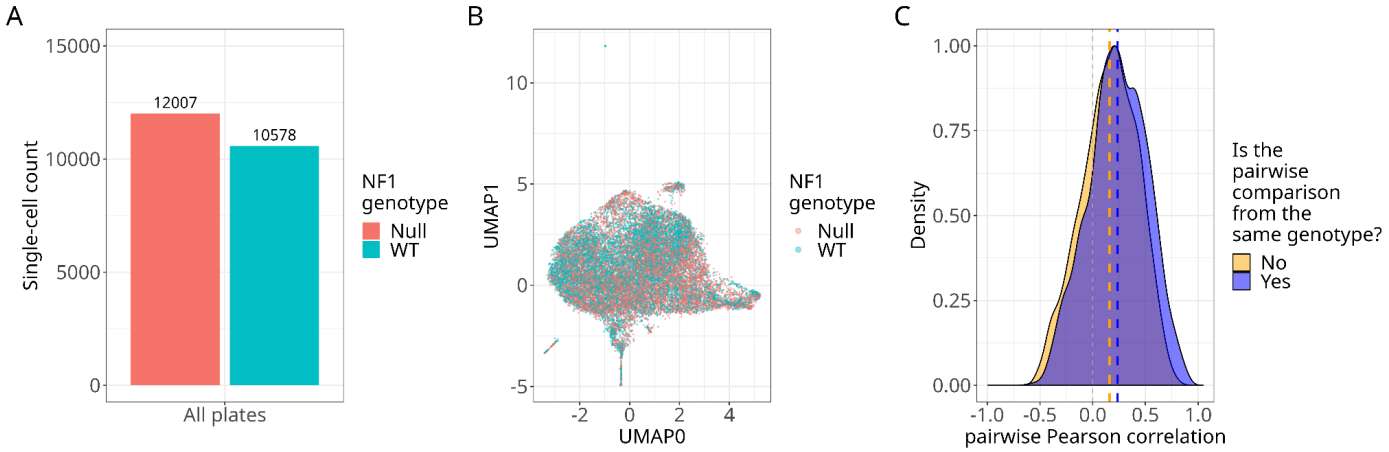

Figure 2. Single-cell and well-level *morphology comparisons between Schwann cell NF1 genotypes show homogeneity, which suggests subtle morphology differences*. (**A**) We acquired and processed a total of 22,585 single Schwann cells for downstream analysis (e.g., machine learning). (**B**) Uniform Manifold Approximation and Projection (UMAP) applied to the morphological features of all single cells demonstrates homogeneity across genotypes. (**C**) Density plot of Pearson correlations of aggregated single cells at the well level shows similar distributions but a higher mean correlation for the same *NF1* genotype.

Predicting *NF1* genotype in isogenic Schwann cells with machine learning

We split the dataset into training and testing (data the model has never seen) sets using a manual method that maximizes the number of single cells per genotype in each data split while maintaining an equivalent number of cells per genotype (see methods for details). This procedure was necessary to ensure our model did not overly emphasize any specific genotype. We trained a penalized logistic regression classifier to predict *NF1* genotype of single Schwann cells, which involved a procedure known as cross-validation to select an optimal model configuration (see methods for details). To compare the model's performance, we created a negative control baseline by independently randomizing morphology features (shuffled baseline), which would indicate any artificial biases. We assessed model performance on the training, cross-validation, and testing sets. Precision-recall curves showed strong performance in predicting *NF1* genotype in the testing set and were much stronger than the shuffled baseline (**Figure 3A**). Confusion matrices also showed a high performance (specificity = 0.79, sensitivity = 0.76; **Figure 3B**). Lastly, we observed 80-85% accuracy in predicting *NF1* genotype (**Figure 3C**).

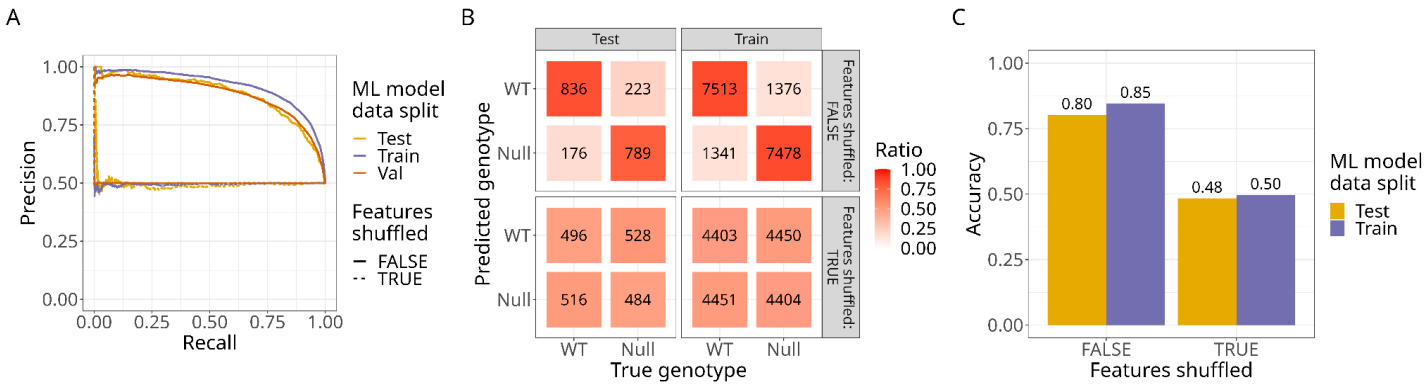

Figure 3. *Logistic regression model predicts NF1 genotype in Schwann cells with high performance*. (**A**) Precision-recall curves comparing the final model applied to shuffled (dashed line) and non-shuffled data (solid line). Applying the model to the shuffled data performed worse than the non-shuffled data, demonstrating a strong biological signal between *NF1* genotypes. (**B**) Confusion matrices from the training and testing sets show higher performance across genotypes in non-shuffled data compared to shuffled data. (**C**) Accuracies demonstrate high performance in predicting both genotypes from the training and testing sets compared to shuffled data.

Multiple organelle morphologies are impacted by *NF1* genotype in Schwann cells

CellProfiler outputs interpretable morphology features, including intensities, textures, granularities, areas, and shapes per organelle.[27] The machine learning model learned from a total of 907 morphology features and assigned weights, or importance scores, per feature. This combination of morphology features represents a high-dimensional signature of how the *NF1* genotype influences cell morphology in otherwise isogenic Schwann cells (**Figure 4A**). Many different cell morphology features are important for distinguishing *NF1* genotypes in Schwann cells. The two most important feature categories were the colocalization of the nucleus and ER in the cells compartment (**Figure 4B**) and the distribution of F-actin in the cytoplasm (**Figure 4C**).

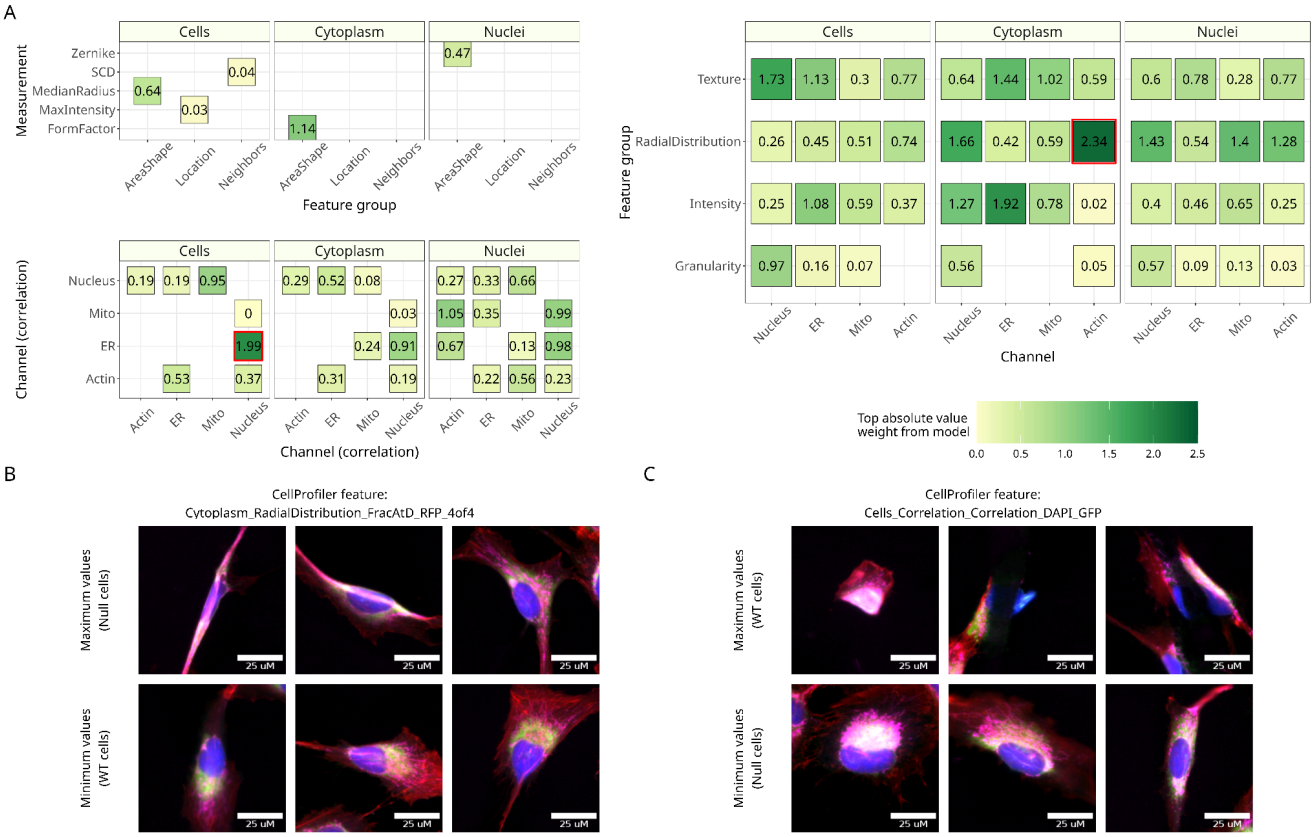

Figure 4. *Significant cell morphology features come from multiple kinds of measurement and across organelles*. (**A**) Top absolute value coefficients demonstrate which measurements/organelles/compartments are important in determining the differences between *NF1* genotypes. Not one feature is important in this prediction; many features in our models are important for making accurate genotype predictions. The red boxes indicate the two most important features based on absolute value. (**B**) Min/max image montage of the top feature from panel A, representing the highest weighted feature for predicting null *NF1* genotype. This shows the visual difference between null cells with the top values of radial distribution in the F-actin cytoskeleton compared to the wildtype cells with the lowest values. The title is the exact CellProfiler feature name. (**C**) Min/max image montage of the second top features from panel A, representing the top feature for predicting wildtype *NF1* genotype. This montage shows the visual difference between the wildtype cells with high correlations between the nucleus and ER compared to the null cells with the lowest values. Both the image montages from panels B and C show composite single-cell images where the colors represent each organelle: blue = nucleus, green = ER, magenta = mitochondria, and red = actin.

Discussion:

Our proof-of-concept experiment demonstrates the feasibility of predicting *NF1* wildtype and null genotypes in Schwann cells using high-content microscopy and machine learning. We achieved balanced accuracy scores of 0.85 for training and 0.80 for testing/holdout data. This performance was substantially better than that of the shuffled datasets, indicating that *NF1* genotype meaningfully influences Schwann cell morphology. These differences are impossible to spot by eye, but we demonstrate that machine learning can detect much more subtle, potentially more important, differences.

Our analysis revealed that a multitude of features from various stained organelles contributed to the model's predictive accuracy. This indicates that the phenotypic markers for *NF1* genotypes are described not only by a few features but also by a complex group of multiple cellular characteristics. Specifically, the nucleus, endoplasmic reticulum (ER), and F-actin cytoskeleton were strongly impacted by *NF1* genotype. For the nucleus and ER, there is a much higher correlation (or colocalization of pixels) of these organelles in wildtype Schwann cells. In the case of F-actin, the total stain intensity was highest at the periphery of the cytoplasm compartment, which was a key predictor of the *NF1* null genotype. This suggests that the loss of neurofibromin expression between these genotypes leads to differences most strongly in these organelles/subcellular components. In previous experiments, fluorescent staining of neurofibromin has implicated differential localization of F-actin or microtubules[35,36] and active transport into the nucleus.[37] Our model corroborates these observations when examining the differences between wildtype and *NF1* null genotypes but also identifies many more morphological differences worthy of followup experimentation.

Quantitative readouts enhance our ability to collect and interpret high-content microscopy data, which is crucial for identifying potential drug treatments from large-scale drug screens. Previous NF1-focused drug screens[17–19] focused on targeting *NF1* deficient cells have utilized simpler readouts, such as cell death or viability by measuring the AC_{50} or IC_{50}, or a specifically targeted readout, such as changes in p-ERK expression. However, phenotypic drug screens can measure much more information, including general cell state[38], drug toxicity[39], and DNA damage[38]. This approach can identify compounds that impact cells phenotypically to go beyond identifying compounds that simply kill cells or change single markers. There have been many applications of machine learning using traditional high-content microscopy approaches (which aggregate single cells into bulk profiles), including predicting drug sensitivity[40] and cell health phenotypes[38]. Recently, single-cell applications have emerged, demonstrating the potential to predict complex phenotypes, such as predicting MitoCheck phenotypes using single-cell nuclear morphology[41] and predicting between pyroptotic and apoptotic cell death states.[42] Based on our work, we can conclude that single-cell quantitative morphology readouts and phenotypic drug screening have significant potential for advancing the study and treatment of NF1.

Our study has some limitations. First, our assay does not include the heterozygous ($NF1^{+/-}$) genotype, which restricts our ability to model the full spectrum of neurofibromin production. This restricts our findings to two of the *NF1* genotypes and prevents us from observing morphological differences at intermediate neurofibromin levels. Our aim was to show proof of concept, and we will include heterozygous Schwann cells in future studies. Additionally, cells were derived from a single, normal patient for the wildtype cell line and used CRISPR-Cas9 to remove *NF1* for the null cell line, which was also immortalized using hTERT, which can change the nature of these cells. This limits our ability to investigate the generalizability of the morphological differences to different biological conditions and other patients. In the future, we will expand and refine our NF1 Schwann cell morphology signature to multiple cell lines with different immortalization strategies. Lastly, it's possible that the biological differences we are observing are influenced not just by the *NF1* genotype but also by other factors. Cells with the null genotype divide more rapidly, which may cause us to capture more cell division-related morphologies compared to

wildtype cells. This increased division rate could also lead to higher cell density, potentially inducing stress-related morphological changes due to high confluence. To reduce any confluence-related effects, we optimized our plating density within each field of view (FOV) and included a covariate of cell count when training machine learning models. These limitations suggest the need for further data collection and method refinement.

In future work, we aim to conduct a phenotypic drug screen using both null and heterozygous Schwann cells to identify targets that shift the cell morphology to make NF1-deficient Schwann cells look healthy. We plan to collect more data to strengthen our high-content morphology signature, including heterozygous NF1 genotypes and Schwann cell lines from different patients and immortalization strategies. This Schwann cell Morphology Atlas will enable us to generate a high-performing machine-learning model that more effectively captures the phenotypic consequences of different neurofibromin levels in Schwann cells. This methodology can be applied to other cell types related to NF1, such as oligodendrocytes, melanocytes, and bone cells. Another potential approach is to develop a modified Cell Painting assay with an additional channel for fluorescent staining of the neurofibromin protein. This channel would provide ground truth for the abundance of neurofibromin at the single-cell level, which is a limitation of bulk-level processes like western blotting. We believe that through this preliminary work, we are paving a path toward using high-content microscopy to discover novel therapeutic agents that can potentially reverse neurofibromas, providing new effective treatment strategies for NF1 patients and their families.

Methods:

Cell Lines

The immortalized human Schwann cell line ipn02.3λ was used as the wildtype cell line. To generate the NF1 null cell line, CRISPR-Cas9 was used, targeting immediately after the initiator methionine in exon 1.[43] Monoclonal knockouts were confirmed by sequencing and western blots confirming loss of NF1 protein. Cells were maintained in DMEM supplemented with Glutamax and 10% FBS.

Cell painting and image acquisition

Cells of each genotype were plated in 96-well black, clear bottom plates (Greiner) in either 10% FBS (Plate A) or 5% FBS (Plates B and C) in DMEM supplemented with Glutamax. Cells were cultured for 24 hours at 37C, 5% CO2. For mitochondria staining, cells were treated with MitoTracker for 30 minutes prior to fixation. After mitochondria staining, cells were fixed and permeabilized, and treated per the Image-IT Cell Painting (Thermofisher). We performed a modified Cell Painting assay that does not include staining for cytoplasmic RNA, nucleoli, and Golgi. Specifically, we used Hoechst (nuclei), 488-tagged Concanavalin A (ER), MitoTracker® Deep Red (mitochondria), and 568 Phalloidin (F-actin). We acquired gray-scale, 16-bit images per FOV. All images were acquired using a four-channel plate reader (Biotek, Cytation5).

Plates A and B utilized 48 wells, with twelve replicate wells per seeding density (500, 1000, 2000, and 4000), with 6 replicates of each NF1 isogenic cell line. Plate C utilized 48 wells, where there are 24 replicate wells per NF1 isogenic cell line.

Whole image quality control

We assessed the quality of the images from all plates to remove those of poor quality. Poor-quality images included large smudges and/or debris, out-of-focus organelles, and over-saturated organelles. We utilized CellProfiler's image quality metrics to decide two image quality features best distinguished between poor and good quality images: Power Log Log Slope (to represent blur) and Percent Maximal (to represent saturation). These were recommended by Caciedo et al. in their paper describing strategies for image-based profiling.[31] We observed that the blur metric makes a Gaussian distribution, where poor-quality images are found at the distribution tails (**Supplemental Figure 3A**). We set the threshold for out-of-focus images in our CellProfiler pipeline as two standard deviations above and below the mean (this process categorized 95% of the data as good quality). As for saturation, we found the distribution skewed towards 0 but with a long tail (**Supplemental Figure 3B**). We set the threshold as two standard deviations above to mean, as any values above are likely oversaturated and of poor quality. After quality control, 968 image sets failed QC (4.7%), and we did not process cells from these images.

Image analysis

We used CellProfiler v4.2.4, a standard software in the image analysis field, to perform our image analysis pipelines.[44] We applied an illumination correction pipeline that ran through each image set (a group of channels at one field of view per well) that passed quality control. This pipeline created an illumination correction function for each channel per image set, applied the function, and saved each corrected image set as TIFF files.

We next applied a segmentation and feature extraction pipeline using CellProfiler. We segmented three compartments for each single cell per image set: nuclei, cells, and cytoplasm. We derived nuclei segmentation using the DAPI channel, cell segmentation from the RFP channel (using the nuclei segmentation as the input to identify cells), and cytoplasm segmentation by subtracting the nuclei from the cell segmentations. These three segmentations are represented by binary masks (0/1) used to extract features from each compartment while ignoring the images' background. We extracted a total of 2,313 features across all compartments per single cell. The pipeline outputs an SQLite database per plate, with each compartment as a table, with all features extracted.

Image-based profiling

To be able to perform downstream analysis and machine learning, we processed the CellProfiler output with an image-based profiling pipeline. First, using CytoTable[32], we converted the SQLite

databases into parquet files. We merge each compartment table based on object number, which leaves one single cell per row with all morphology features. We next used pycytominer[33], a bioinformatics software for processing image-based profiles, to complete the processing. First, we performed annotation where we combined metadata per well from a plate map with every single cell (e.g., genotype, plate, etc.). After annotation, we normalized the cell morphology features using the standard scalar method, which transforms data to zero mean with unit variance. Lastly, we performed feature selection on the normalized data, which removes non-informative and redundant features. We used four operations in feature selection: variance threshold, correlation threshold, blocklist, and drop NaN columns. We set the variance threshold as the default frequency cutoff of 0.05, which will remove features with low variance across all single cells. We set the correlation threshold as the default Pearson correlation threshold of 0.9, where we removed one of the highly correlated features by selecting the feature with the lowest absolute value correlation to all the other features. We removed features included in the blocklist default file as set by pycytominer. Lastly, we removed features with at least one NaN value by setting the na_cutoff parameter as 0. For the machine learning model, we took the intersection of the features selected across plates, leaving 907 common features. After feature selection, we performed aggregation, taking the average values of each morphology feature per well. We segmented 11,286 single cells from 48 wells for Plate A, 5,506 from 48 wells for Plate B, and 5,793 single cells from 48 wells for Plate C. We performed aggregation to the well-level post-feature selection to assess the correlations between genotypes. We used single-cell profiles for machine learning, which included heterogeneity, while aggregated profiles summarized the profiles to reduce complexity but removed outliers that could be interesting biology.

Machine learning: Data splitting and sampling

Before training the final machine learning model, we first optimized our dataset for predicting genotypes. To avoid bias toward either *NF1* genotype, we first balanced the distribution of classes. Prior to balancing, we created training and testing sets. Cells from the testing set came from different wells than cells from the training set. This ensured we measured the machine learning model's effective predictive ability generalizing to new cell populations, eliminating the possibility of cells influencing neighboring cell morphologies between data splits. Ultimately, this procedure prevents model performance inflation by preventing data leakage. We manually split the testing and training wells to achieve the approximate ratio of 90% training cells to 10% testing cells. We then randomly downsampled the training and testing sets to an equivalent number of cells in each data split by genotype.[45]

Machine learning: Model training and evaluation

We developed an interpretable machine-learning approach to identify important morphology features responsible for discerning *NF1* genotypes. We trained an NF1 model using an L2-regularized logistic regression architecture. L2 regularization reduces overfitting without encouraging sparsity of morphology weights after feature selection.[46] We determined the optimal

inverse regularization strength ($\lambda = C^{-1}$) by performing a random search on the class-balanced training data with a stratified 8-fold cross-validation. We evaluated the accuracy on the holdout cross-validated data of 500 logistic regression models, each with an inverse regularization strength $\lambda \sim U(0, 200)$, and we chose hyperparameters that maximized this accuracy. We then computed validation metrics from all testing folds, which have previously been shown to reduce bias.[46] To compare our results to a negative control baseline, we randomized each feature independently for each dataset and then evaluated each of these augmented datasets. After this randomization, we retrained the model on the entire training split, and evaluated the performance on the training and testing splits.

Data availability:

Datasets containing the original images can be found on figshare at https://figshare.com/projects/NF1_Schwann_Cell_Genotype_Cell_Painting_Assay/161620.[47–51] Code to download datasets, perform image analysis with CellProfiler, and image-based profiling with CytoTable and pycytominer is available on GitHub at https://github.com/WayScience/nf1_cellpainting_data.[52] Code to perform all analyses (EDA, machine learning model training, validation, and figure making) is available at https://github.com/WayScience/nf1_schwann_cell_morphology_signature.[53]

Acknowledgements:

We would like to thank Dave Bunten, Mike Lippincott, Erik Serrano, and Roshan Kern for their contribution to code reviews. S.J.B. was also funded in part by the National Human Genome Research Institute (NHGRI) under award #T32HG010464.

Funding:

This work was funded by a Department of Defense (DoD) Congressionally Directed Medical Research Programs (CDMRP) Neurofibromatosis Research Program (NFRP) Early Investigator Research Award (EIRA) HT9425-23-1-0831 to S.J.B.

Conflicts of interest:

MMH and HS are employees of Infixion Bioscience. GPW serves on the scientific advisory board of Infixion Bioscience.

References:

1. Wang, W. *et al.* Impacts of NF1 Gene Mutations and Genetic Modifiers in Neurofibromatosis Type 1. *Front. Neurol.* **12**, 704639 (2021).
2. Pemov, A., Park, C., Reilly, K. M. & Stewart, D. R. Evidence of perturbations of cell cycle

and DNA repair pathways as a consequence of human and murine NF1-haploinsufficiency. *BMC Genomics* **11**, 194 (2010).
3. Johnson, K. J. *et al.* Development of an international internet-based neurofibromatosis Type 1 patient registry. *Contemp. Clin. Trials* **34**, 305–311 (2013).
4. Legius, E. & Brems, H. Genetic basis of neurofibromatosis type 1 and related conditions, including mosaicism. *Childs. Nerv. Syst.* **36**, 2285–2295 (2020).
5. Rossi, S. *et al.* Neurofibromin C terminus-specific antibody (clone NFC) is a valuable tool for the identification of NF1-inactivated GISTs. *Mod. Pathol.* **31**, 160–168 (2018).
6. Serra, E. *et al.* Confirmation of a double-hit model for the NF1 gene in benign neurofibromas. *Am. J. Hum. Genet.* **61**, 512–519 (1997).
7. Colman, S. D., Williams, C. A. & Wallace, M. R. Benign neurofibromas in type 1 neurofibromatosis (NF1) show somatic deletions of the NF1 gene. *Nat. Genet.* **11**, 90–92 (1995).
8. Park, S.-J. *et al.* Serum biomarkers for neurofibromatosis type 1 and early detection of malignant peripheral nerve-sheath tumors. *BMC Med.* **11**, 109 (2013).
9. Cannon, A. *et al.* Cutaneous neurofibromas in Neurofibromatosis type I: a quantitative natural history study. *Orphanet J. Rare Dis.* **13**, 31 (2018).
10. Needle, M. N. *et al.* Prognostic signs in the surgical management of plexiform neurofibroma: the Children's Hospital of Philadelphia experience, 1974-1994. *J. Pediatr.* **131**, 678–682 (1997).
11. Higham, C. S. *et al.* The characteristics of 76 atypical neurofibromas as precursors to neurofibromatosis 1 associated malignant peripheral nerve sheath tumors. *Neuro. Oncol.* **20**, 818–825 (2018).
12. Lim, Z., Gu, T. Y., Tai, B. C. & Puhaindran, M. E. Survival outcomes of malignant peripheral nerve sheath tumors (MPNSTs) with and without neurofibromatosis type I (NF1): a meta-analysis. *World J. Surg. Oncol.* **22**, 14 (2024).
13. Gross, A. M. *et al.* Selumetinib in Children with Inoperable Plexiform Neurofibromas. *N. Engl. J. Med.* **382**, 1430–1442 (2020).
14. Sharawat, I. K., Panda, P. K., Sihag, R. K., Panda, P. & Dawman, L. Efficacy and safety profile of selumetinib in symptomatic inoperable plexiform neurofibromas. *J. Neurosurg. Sci.* **66**, 501–510 (2022).
15. Gross, A. M. *et al.* Selumetinib in children with neurofibromatosis type 1 and asymptomatic inoperable plexiform neurofibroma at risk for developing tumor-related morbidity. *Neuro. Oncol.* **24**, 1978–1988 (2022).
16. Frost, M. *et al.* Rationale for haploinsufficiency correction therapy in neurofibromatosis type 1. *J. Transl. Genet. Genom.* **6**, 403–428 (2022).
17. Bouley, S. J. *et al.* Chemical genetic screens reveal defective lysosomal trafficking as synthetic lethal with NF1 loss. *J. Cell Sci.* **137**, (2024).
18. See, W. L., Tan, I.-L., Mukherjee, J., Nicolaides, T. & Pieper, R. O. Sensitivity of glioblastomas to clinically available MEK inhibitors is defined by neurofibromin 1 deficiency. *Cancer Res.* **72**, 3350–3359 (2012).
19. Maertens, O. *et al.* Elucidating distinct roles for NF1 in melanomagenesis. *Cancer Discov.* **3**, 338–349 (2013).
20. Vincent, F. *et al.* Phenotypic drug discovery: recent successes, lessons learned and new directions. *Nat. Rev. Drug Discov.* **21**, 899–914 (2022).
21. Way, G. P., Sailem, H., Shave, S., Kasprowicz, R. & Carragher, N. O. Evolution and impact of high content imaging. *SLAS Discov* **28**, 292–305 (2023).
22. Miller, S. J. *et al.* Large-scale molecular comparison of human schwann cells to malignant peripheral nerve sheath tumor cell lines and tissues. *Cancer Res.* **66**, 2584–2591 (2006).
23. Ferrer, M. *et al.* Pharmacological and genomic profiling of neurofibromatosis type 1 plexiform neurofibroma-derived schwann cells. *Sci Data* **5**, 180106 (2018).

24. Suppiah, S. *et al.* Multiplatform molecular profiling uncovers two subgroups of malignant peripheral nerve sheath tumors with distinct therapeutic vulnerabilities. *Nat. Commun.* **14**, 2696 (2023).
25. Kim, H. A., Rosenbaum, T., Marchionni, M. A., Ratner, N. & DeClue, J. E. Schwann cells from neurofibromin deficient mice exhibit activation of p21ras, inhibition of cell proliferation and morphological changes. *Oncogene* **11**, 325–335 (1995).
26. Bray, M.-A. *et al.* Cell Painting, a high-content image-based assay for morphological profiling using multiplexed fluorescent dyes. *Nat. Protoc.* **11**, 1757–1774 (2016).
27. Carpenter, A. E. *et al.* CellProfiler: image analysis software for identifying and quantifying cell phenotypes. *Genome Biol.* **7**, R100 (2006).
28. Caicedo, J. C. *et al.* Cell Painting predicts impact of lung cancer variants. *Mol. Biol. Cell* **33**, ar49 (2022).
29. Li, H., Chang, L.-J., Neubauer, D. R., Muir, D. F. & Wallace, M. R. Immortalization of human normal and NF1 neurofibroma Schwann cells. *Lab. Invest.* **96**, 1105–1115 (2016).
30. Singh, S., Bray, M.-A., Jones, T. R. & Carpenter, A. E. Pipeline for illumination correction of images for high-throughput microscopy. *J. Microsc.* **256**, 231–236 (2014).
31. Caicedo, J. C. *et al.* Data-analysis strategies for image-based cell profiling. *Nat. Methods* **14**, 849–863 (2017).
32. Bunten, D., Alquaddoomi, F., Serrano, E., & Way, G. *CytoTable*. (Github).
33. Serrano, E. *et al.* Reproducible image-based profiling with Pycytominer. *ArXiv* (2024).
34. McInnes, L., Healy, J. & Melville, J. UMAP: Uniform Manifold Approximation and Projection for Dimension Reduction. *arXiv [stat.ML]* (2018).
35. Li, C., Cheng, Y., Gutmann, D. A. & Mangoura, D. Differential localization of the neurofibromatosis 1 (NF1) gene product, neurofibromin, with the F-actin or microtubule cytoskeleton during differentiation of telencephalic neurons. *Brain Res. Dev. Brain Res.* **130**, 231–248 (2001).
36. Gregory, P. E. *et al.* Neurofibromatosis type 1 gene product (neurofibromin) associates with microtubules. *Somat. Cell Mol. Genet.* **19**, 265–274 (1993).
37. Vandenbroucke, I., Van Oostveldt, P., Coene, E., De Paepe, A. & Messiaen, L. Neurofibromin is actively transported to the nucleus. *FEBS Lett.* **560**, 98–102 (2004).
38. Way, G. P. *et al.* Predicting cell health phenotypes using image-based morphology profiling. *Mol. Biol. Cell* **32**, 995–1005 (2021).
39. Nyffeler, J. *et al.* Bioactivity screening of environmental chemicals using imaging-based high-throughput phenotypic profiling. *Toxicol. Appl. Pharmacol.* **389**, 114876 (2020).
40. Kelley, M. E. *et al.* High-content microscopy reveals a morphological signature of bortezomib resistance. *bioRxiv* (2023) doi:10.1101/2023.05.02.539137.
41. Tomkinson, J., Kern, R., Mattson, C. & Way, G. P. Toward generalizable phenotype prediction from single-cell morphology representations. *bioRxiv* 2024.03.13.584858 (2024) doi:10.1101/2024.03.13.584858.
42. Lippincott, M. J. *et al.* A morphology and secretome map of pyroptosis. *bioRxiv* 2024.04.26.591386 (2024) doi:10.1101/2024.04.26.591386.
43. Zhang, T., Han, T., Dong, Z., Li, C. & Lu, W. Characterization of Two Loss-of-Function NF1 Variants in Chinese Patients and Potential Molecular Interpretations of Phenotypes. *Front. Genet.* **12**, 660592 (2021).
44. Stirling, D. R. *et al.* CellProfiler 4: improvements in speed, utility and usability. *BMC Bioinformatics* **22**, 433 (2021).
45. Lee, W. & Seo, K. Downsampling for Binary Classification with a Highly Imbalanced Dataset Using Active Learning. *Big Data Research* **28**, 100314 (2022).
46. Forman, G. & Scholz, M. Apples-to-apples in cross-validation studies: pitfalls in classifier performance measurement. *SIGKDD Explor. Newsl.* **12**, 49–57 (2010).
47. Tomkinson, J., Mattson-Hoss, M., Sarnoff, H. & Way, G. Plate 3 and Plate 3’ (prime).

https://doi.org/10.6084/m9.figshare.22592890.v1 (2023).
48. Tomkinson, J., Mattson-Hoss, M., Sarnoff, H. & Way, G. Plate 5. https://doi.org/10.6084/m9.figshare.26759914.v1 (2024).
49. Tomkinson, J., Mattson-Hoss, M., Sarnoff, H. & Way, G. Plate 1. https://doi.org/10.6084/m9.figshare.22233292.v1 (2023).
50. Tomkinson, J., Mattson-Hoss, M., Sarnoff, H. & Way, G. Plate 2. https://doi.org/10.6084/m9.figshare.22233700.v1 (2023).
51. Tomkinson, J., Mattson-Hoss, M., Sarnoff, H. & Way, G. Plate 4. https://doi.org/10.6084/m9.figshare.23671056.v1 (2023).
52. Tomkinson, J., Mattson, C. Way, G., Serrano, E. *nf1_schwann_cell_painting_data*. doi:10.5281/zenodo.13345304.
53. Mattson, C., Tomkinson, J., Way, G. *WayScience/nf1_schwann_cell_morphology_signature: v1.1 - Manuscript Updates*. doi:10.5281/zenodo.13694800.